Characteristic plateau in the L_1-subshell ionization cross section of Ag induced by proton collisions

M. Kavčič[1] and Ž. Šmit[1,2]
[1]*J. Stefan Institute, Jamova 39, SI-1000 Ljubljana, Slovenia*
[2]*Faculty of Mathematics and Physics, University of Ljubljana, Jadranska 19, SI-1000 Ljubljana, Slovenia*
(Received 13 July 2009; published 3 December 2009)

A characteristic dependence of the proton-induced 2*s* subshell ionization cross section generated by the nodal structure of the 2*s* wave function was probed via high-resolution measurements of the $L\beta_3$ (L_1-M_3) and $L\beta_6$ (L_3-N_1) x-ray lines of Ag. The intensity ratio of the measured lines depends strongly on the proton energy exhibiting a pronounced maximum around 0.4 MeV. The experimental intensities are critically compared to the theoretically predicted values. The latter were obtained using the ionization cross sections calculated within the semiclassical approximation employing hydrogenlike and Dirac-Fock electron wave functions.

DOI: 10.1103/PhysRevA.80.062706 PACS number(s): 34.50.Fa, 32.30.Rj, 32.70.−n

I. INTRODUCTION

The process of inner-shell ionization induced by ion-atom collisions is of basic importance for our understanding of interaction of ions with matter and has been studied extensively over the last few decades both experimentally and theoretically. Based on these numerous studies large compilations of cross-section data have been built especially for the *K* and *L* shells ionized by protons and He ions [1,2]. Generally a good agreement between the measured and calculated data was found for the *K* and total *L* shell ionization cross sections, while some systematic discrepancies were observed for the *L*-subshell ionization cross sections [3] and later also for *L*-subshell ionization cross sections induced by heavy ions [4,5]. Most of the experimental ionization cross sections were obtained from the measured x-ray fluorescence yields. In case of *L*,*M* subshell ionization this approach has an additional limitation, which is a complex x-ray spectrum composed of several overlapping spectral lines due to transitions to different subshells. Especially for low and mid-*Z* elements the energy resolution of energy dispersive detectors is not sufficient to resolve completely the partial subshell fluorescence contributions, limiting such studies to the total x-ray production cross sections. Most of the work on ion-induced inner-shell ionization is therefore focused on the collection of the ionization cross sections, which are for *L*,*M* subshells of low and mid-*Z* elements even additionally limited to the total *L*,*M* shell ionization cross sections. In order to advance the field further we need to look for alternative approaches and fundamental effects, which could provide a base for a more stringent comparison with theory.

While a smooth monotonic rise of the inner-shell ionization cross section with increasing projectile's energy is usually expected for charged particle ionization at low impact energies, the energy dependence of the photoionization cross section may exhibit a characteristic Cooper minimum [6], which is due to the node of the initial-state radial wave function. As a result, the dipole matrix element for a particular channel changes sign (goes through zero) at a certain photon energy producing a characteristic minimum in the cross section. Especially the position of this minimum represents one of the most sensitive dynamical quantities in photoionization. Since such a Cooper minimum represents a matrix element effect, similar behavior could be expected also for charged particle ionization and excitation. In fact, for atomic excitations induced by inelastic scattering of fast electrons a minimum of the generalized oscillator strength at large momentum transfers was already predicted a long time ago [7,8]. For the inner-shell ionization induced by ion collisions the total ionization cross section is usually studied. In this case, integration over the energy of the ejected electron smears out the minimum in the generalized oscillator strength for a given energy of the ejected inner-shell electron, but it produces a plateau in the total subshell ionization cross section [9]. For the 2*s* subshell ionization cross section of Au induced in collisions with protons and helium ions such a plateau was also confirmed experimentally [10].

In our recent work [11], wavelength dispersive x-ray spectroscopy was used successfully to separate partial *L*-subshell contributions also in case of a mid-*Z* element such as Pd (Z=46). It was shown that the plateau in the calculated 2*s* subshell ionization cross section generated by the nodal structure of the 2*s* wave function is especially pronounced in the ratio of the L_3 and L_1 subshell ionization cross sections producing a characteristic maximum. This maximum can be probed directly via high-resolution measurements of the corresponding L_1 and L_3 x-ray lines. Since the nature of this maximum reflects the transition matrix elements, we can expect it to be very sensitive to the shape of the initial state wave function, thus representing a severe test for theoretical calculations.

In this work we report about a detailed experimental and theoretical studies of the characteristic structure of the proton induced 2*s* subshell ionization of Ag. Wavelength dispersive x-ray spectroscopy was employed to measure the intensity ratio of particular proton induced L_3- and L_1-subshell x-ray lines while changing the energy of the impinging protons in small energy steps within the interval where the maximum is expected. The measured dependence of the $L\beta_6$ and $L\beta_3$ intensity ratio on the proton energy is compared with results of detailed calculations confirming the sensitivity of the model to the choice of the wave function used for the description of the initial state. The experimental approach presented here could be applied to a variety of other targets and projectiles

providing valuable data, which could stimulate theoretical approaches in the field of ion-atom collisions.

II. EXPERIMENT

Measurements were carried out at the Microanalytical Centre (MIC) of the Jožef Stefan Institute in Ljubljana. Protons were accelerated by a 2 MV tandem accelerator. The incident proton beam with a size of 8×8 mm^2 and a current up to a few μA was impinging on a thick pure Ag target tilted at 45° with respect to the incoming proton beam. The target $L\beta_{3,4,6}$ x-ray fluorescence was measured in the direction perpendicular to the incoming proton beam using a crystal spectrometer in Johansson geometry with a 500 mm Rowland circle radius. The first-order reflection of a Si(111) crystal was used and the diffracted photons were detected with a thermoelectrically cooled (−40 °C) charge coupled device (CCD) camera with 22.5×22.5 μm^2 pixel size. The overall energy resolution of the spectrometer was below 1 eV. In order to use the whole proton current dispersed over a rather large spot on the target surface, the target was placed well inside the Rowland circle at a distance of 27 cm in front of the crystal. Using the whole length of the CCD camera the full $L\beta_{3,4,6}$ x-ray fluorescence spectrum was measured simultaneously at a fixed detector position. A series of 21 x-ray emission spectra in total was recorded at proton energies of 0.2–2.0 MeV, with majority of the collected spectra taken in the 0.2–0.8 MeV proton energy range, with 0.05 MeV energy steps. The nominal proton beam energies given by the terminal voltage were converted into more accurate values by the calibration procedure based on known energies of the nuclear $p\gamma$ resonances in F and Al. The acquisition time for each spectrum depended heavily on the proton energy. While at 2.0 MeV the total acquisition time was only 750 s it increased drastically at low proton energies. As the cross section diminishes very rapidly the total acquisition times at lowest proton energies were up to 14 h.

III. DATA ANALYSIS

Fig. 1 shows three $L\beta_{3,4,6}$ x-ray fluorescence spectra recorded at three different proton energies. While the $L\beta_{3,4}$ doublet represents the fluorescence from the L_1 subshell, the $L\beta_6$ line at a higher x-ray energy represents the fluorescence from the L_3 ionized subshell. A plateau in the $2s$ ionization cross section, which is predicted by the calculations, should be reflected in a pronounced maximum of the σ_{L3} and σ_{L1} cross-section ratio as shown in the inset of Fig. 2. This characteristic dependence should be manifested directly in the intensity ratio of the $L\beta_3$ and $L\beta_6$ lines as they are directly related to the ionization of the L_1 and L_3 subshells, respectively. In fact a strong dependence of this ratio on the proton energy is observed clearly from the spectra presented in Fig. 1.

In order to extract the $L\beta_3$ and $L\beta_6$ line intensities each spectrum was analyzed by a least square fitting procedure. Since the natural linewidths [$\Gamma(L_1$-$M_3)$=6.35 eV and $\Gamma(L_3$-$N_1)$=6.55 eV [12]] are much larger than our experimental resolution the measured lines were approximated

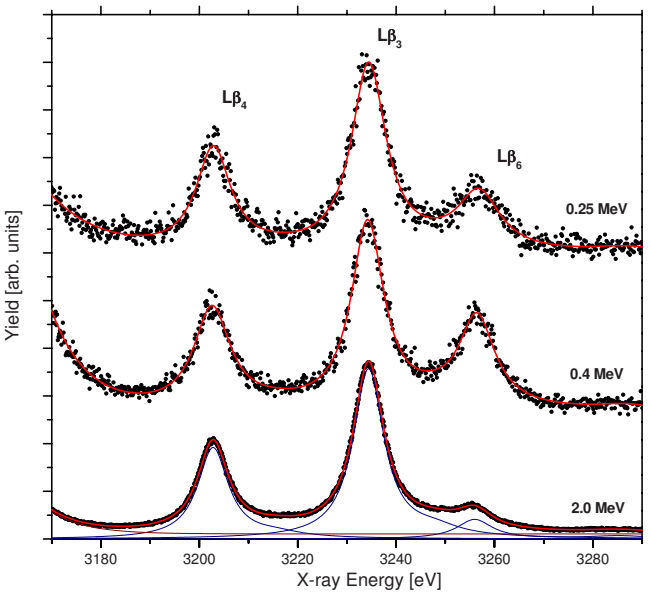

FIG. 1. (Color online) High-resolution proton induced $L\beta_3$ (L_1-M_3), $L\beta_4$ (L_1-M_2), and $L\beta_6$ (L_3-N_1) x-ray emission spectra of Ag measured at three different proton energies. The full line corresponds to the fit; separate components of the fitting model are presented for the spectrum taken with 2 MeV protons. The intensity ratio of the $L\beta_6$ and $L\beta_3$ x-ray lines clearly varies with the proton energy.

with Lorentzians. An additional weak component was added on the high-energy side of each diagram line in order to account for the satellite contributions due to the LM double ionization. An exponential decay was added to the constant background to account for the tail of the $L\beta_1$ diagram line contributing on the low energy side of our measured spectra. Such a fitting model described well the measured spectra (see Fig. 1). Since variations in the crystal reflectivity and the efficiency of the CCD detector within the measured x-ray spectral range were less than 1%, these effects were ne-

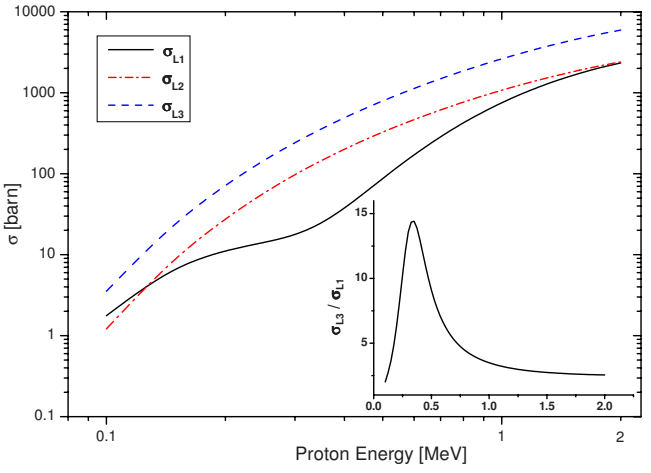

FIG. 2. (Color online) Theoretical L-subshell ionization cross sections of Ag calculated with the semiclassical approximation using Dirac-Fock electron wave functions. Shown in the inset is the ratio of the L_3 and L_1 subshell ionization cross sections which exhibits a pronounced peak at low proton energies.

glected in our analysis. The final intensity ratio of the $L\beta_6$ and $L\beta_3$ diagram lines as a function of the proton energy is presented in Fig. 3. The error bars represent the fitting errors.

The experimental intensities are not directly proportional to the L subshell ionization cross sections since one needs to consider the stopping of the projectiles in the target as well as absorption of x-rays on their way out. Once we have calculated the L-subshell ionization cross sections the final intensities of the $L\beta_3$ and $L\beta_6$ lines are given by the following equations:

$$Y_{L\beta_3} \propto \omega_{L_1} \frac{\Gamma_{L\beta_3}}{\Gamma_{L_1}^{Rad}} \int_0^R \sigma_{L_1}^I(E(x)) e^{-\mu_{L\beta_3} x} dx, \quad (1)$$

$$Y_{L\beta_6} \propto \omega_{L_3} \frac{\Gamma_{L\beta_6}}{\Gamma_{L_3}^{Rad}} \left[\int_0^R \sigma_{L_3}^I(E(x)) e^{-\mu_{L\beta_6} x} dx + f_{23} \int_0^R \sigma_{L_2}^I(E(x)) e^{-\mu_{L\beta_6} x} dx + (f_{12} f_{23} + f_{13} + f'_{13}) \int_0^R \sigma_{L_1}^I(E(x)) e^{-\mu_{L\beta_6} x} dx \right], \quad (2)$$

where $E(x)$ being the proton energy as a function of the penetration depth, R is the range of protons in the target, σ^I is the L- subshell ionization cross sections, $\Gamma_{L\beta}/\Gamma_L^{Rad}$ is the relative emission rate for a particular $L\beta$ radiative transition, f_{ij} are the Coster-Kronig yields, and $\omega_{1,3}$ are the fluorescence yields for the L_1 and L_3 subshells, respectively. In our calculations, the integrations in Eqs. (1) and (2) were converted into the energy integrals using the well-known transformation $dx = dE/S(E)$, with S being the proton stopping power given by [13]. The experimental values of Jitschin *et al.* [14] and Auerhammer *et al.* [15] were used for the Coster-Kronig coefficients and the L subshell fluorescence yields of Ag, respectively, and the theoretical radiative transition probabilities as given by Scofield [16].

IV. RESULTS AND DISCUSSION

When the proton impact energy is only a few tenths of MeV, protons are significantly decelerated and deflected in the field of the nucleus. Therefore, we have calculated the L-subshell ionization cross sections within the semiclassical approximation (SCA) [17], accounting for this deflection by the hyperbolic trajectories of the projectiles as classical particles. The influence of the electron cloud, partly screening the field of the nucleus, was taken into account by increasing slightly the projectile impact energy [18,19]. The calculation was made with the screened hydrogenic Dirac wave functions, obeying the principle of Bethe [20]. In this approach, the screening of outer shell electrons is approximated by a constant potential. The continuum wave functions near the ionization threshold are then calculated for virtually bound states with a negative energy, which agree very well with the wave functions calculated for the Herman-Skillman potential [21]. In order to probe the sensitivity of the characteristic peak on the type of the electron wave functions, we have also

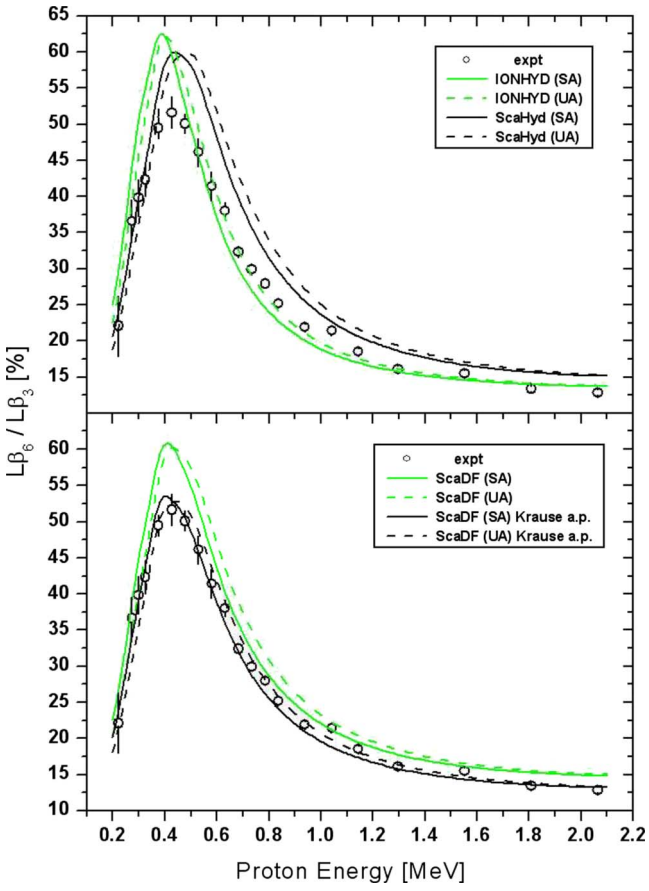

FIG. 3. (Color online) (Top) Experimental $L\beta_6$ and $L\beta_3$ relative intensities compared with the theoretical values calculated within the semiclassical (SCA) model employing two different types of hydrogenic wave functions. Two sets of curves represent values calculated within the SA and UA model. (Bottom) Experimental intensities compared with the SCA calculation using Dirac-Fock wave functions. The theoretical curve employing the semiempirical values of the atomic parameters (L-subshell fluorescence and Coster-Kronig yields) as given by Krause [26] is in excellent agreement with the experiment.

calculated the L-subshell ionization cross sections using the IONHYD code [22] that still employs the SCA model but uses a slightly different hydrogenic approximation. The continuum wave functions in this model do not obey the principle of Bethe but correspond to the situation far from the atom. The relative intensities of the $L\beta_6$ and $L\beta_3$ diagram lines calculated according to Eqs. (1) and (2) using both sets of calculated ionization cross-sections are compared to the experimental intensities in the upper part of Fig. 3 confirming the sensitivity of the characteristic peak on the electron wave functions as both calculated maxima differ by approximately 55 keV.

For an accurate cross-section calculation, the modeling has to go beyond the first-order theory. The lowest-order term, obtained from the coupled-channel model, points to the increased binding energy of the bound state at adiabatic collisions [23]. Simple physical arguments proposed by several authors led to the united-atom (UA) concept which imposes shrinking of the atomic wave function due to the presence of

the positively charged projectile. Although the united-atom limit at extreme adiabatic collisions is never reached as the formation of quasimolecular orbitals causes the cross section to oscillate [24], we have complemented the calculations described above [separated-atom (SA) approximation] also with the ionization cross sections calculated in the united-atom approach as it represents the other extreme limit of the secondary effects.

Comparison of the intensities calculated for the hydrogenic wave functions with the experimental values is presented in the upper part of Fig. 3. While our semiclassical calculations (ScaHyd) overestimate the position of the characteristic peak, this position is underestimated in the IONHYD calculation. A small systematic shift of this position going from the separated atom to the united-atom description is also observed, irrespective of the wave functions used.

Since we were not able to reproduce accurately the position of the characteristic peak using hydrogenic wave functions, we have replaced them with more realistic Dirac-Fock (DF) wave functions and repeated the SCA ionization cross-section calculations. The DF bound-state wave functions were calculated by the GRASP package [25]. The continuum wave functions, which only smoothly oscillate in the integration region, are less critical and we retained the hydrogenic values. Also in this case the cross-section calculations within the separated-atom and united-atom concept were performed. These ionization cross sections were then used to calculate the relative intensities, which are presented in the bottom part of Fig. 3, where they are also compared with the experimental values. The position of the calculated maximum matches well the experimental one. Comparison of the separated-atom and united-atom description indicates that the experimental values are situated between the two curves. This is expected as the projectile velocities at energies around the characteristic peak reach values around 0.7 (in atomic units) which does not favor either of the two models representing both limiting cases.

Up to this point we have focused our attention to the calculated position of the characteristic peak only and not to the absolute values of the $L\beta_6$ and $L\beta_3$ line intensity ratios, which are overestimated compared to the experimental intensity ratios by approximately 10%. In contrast to the position of the characteristic peak, the calculated intensity ratios do not differ significantly for calculations employing different wave functions, as shown in Fig. 3. The difference might be therefore attributed to the uncertainty of the atomic parameters (L subshell fluorescence and Coster-Kronig yields) used in the calculation of the $L\beta_6$ and $L\beta_3$ line intensities [Eqs. (1) and (2)]. In our analysis we have used experimental values that were reported for Ag in Refs. [14,15]. The available experimental data was one of the reasons for choosing Ag for our study. Generally, for the fluorescence yields and Coster-Kronig coefficients semiempirical data of Krause [26] are most commonly used. If we compare only the L-subshell fluorescence yields of Ag, the experimental ω_{L3} value of Auerhammer *et al.* [15] (0.058 ± 0.010) used in our calculation is consistent within the reported error with the semiempirical value of Krause [26] (0.052 ± 0.008), whereas the two ω_{L1} values match each other (0.016 ± 0.004). The same holds also for the experimental Coster-Kronig coefficients of Ag reported by Jitschin *et al.* [14], which are within experimental uncertainties consistent with the semiempirical values given by Krause [26], but the absolute values used in our calculations differ significantly as in the case of fluorescence yields. In order to confirm the origin of the systematic discrepancies between the experimental and calculated intensity ratios we have recalculated the relative intensities of the $L\beta_6$ and $L\beta_3$ diagram lines according to Eqs. (1) and (2) employing cross sections calculated with the DF wave functions, but using semiempirical data of Krause [26] for the L-subshell fluorescence yields as well as Coster-Kronig coefficients. Results of these calculations, which are presented in the lower part of Fig. 3, are in excellent agreement with the experimental data supporting therefore the semiempirical Coster-Kronig and fluorescence L shell yields as given by Krause [26].

V. SUMMARY AND CONCLUSIONS

The intensity ratio of the $L\beta_6$ and $L\beta_3$ x-ray lines of Ag bombarded by 0.2–2 MeV protons was measured employing the wavelength dispersive spectroscopy. Our experiment confirmed the characteristic peak at low proton energies which reflects the nodal structure of the $2s$ wave function. It was further demonstrated that the position of the peak is very sensitive to the wave functions used providing therefore a stringent test for the theory. The calculated intensities employing the Dirac-Fock wave functions and the semiempirical values for the L-subshell fluorescence and Coster Kronig yields given by Krause [26] are in excellent agreement with the experimental values.

ACKNOWLEDGMENTS

The authors would like to thank M. Žitnik for calculating the DF electron wave functions and J. Hoszowska for checking the paper. This work was supported by the Slovenian Ministry of Higher Education, Science, and Technology (research program P1-0112).

[1] H. Paul and J. Sacher, At. Data Nucl. Data Tables **42**, 105 (1989).
[2] I. Orlić, C. H. Sow, and S. M. Tang, At. Data Nucl. Data Tables **56**, 159 (1994).
[3] E. Braziewicz *et al.*, J. Phys. B **24**, 1669 (1991).
[4] M. Pajek *et al.*, Phys. Rev. A **68**, 022705 (2003).
[5] G. Lapicki, A. C. Mandal, S. Santra, D. Mitra, M. Sarkar, D. Bhattacharya, P. Sen, L. Sarkadi, and D. Trautmann, Phys. Rev. A **72**, 022729 (2005).
[6] J. W. Cooper, Phys. Rev. **128**, 681 (1962).

[7] Y.-K. Kim, M. Inokuti, G. E. Chamberlain, and S. R. Mielczarek, Phys. Rev. Lett. **21**, 1146 (1968).
[8] R. Padma and P. C. Deshmukh, Phys. Rev. A **46**, 2513 (1992).
[9] S. T. Manson and A. Msezane, J. Phys. B **8**, L5 (1975).
[10] S. Datz, J. L. Duggan, L. C. Feldman, E. Laegsgaard, and J. U. Andersen, Phys. Rev. A **9**, 192 (1974).
[11] M. Kavčič and Ž. Šmit, Phys. Rev. A **79**, 052708 (2009).
[12] J. L. Campbell and T. Papp, At. Data Nucl. Data Tables **77**, 1 (2001).
[13] J. F. Ziegler, Nucl. Instrum. Methods Phys. Res. B **219-220**, 1027 (2004).
[14] W. Jitschin, R. Stötzel, T. Papp, and M. Sarkar, Phys. Rev. A **59**, 3408 (1999).
[15] J. Auerhammer, H. Genz, and A. Richter, Z. Phys. D: At., Mol. Clusters **7**, 301 (1988).
[16] J. H. Scofield, Phys. Rev. A **10**, 1507 (1974).
[17] Ž. Šmit and I. Orlić, Phys. Rev. A **50**, 1301 (1994).
[18] A. Jakob, F. Rösel, D. Trautmann, and G. Baur, Z. Phys. A **309**, 13 (1982).
[19] Ž. Šmit, Phys. Rev. A **53**, 4145 (1996).
[20] H. A. Bethe, *Handbuch der Physik* (Springer, Berlin, 1933), Vol. 24, p. 172–174.
[21] L. Kocbach, J. M. Hansteen, and R. Gundersen, Nucl. Instrum. Methods Phys. Res. B **169**, 281 (1980).
[22] D. Trautmann and F. Rösel, Nucl. Instrum. Methods Phys. Res. B **169**, 259 (1980).
[23] W. Brandt and G. Lapicki, Phys. Rev. A **10**, 474 (1974).
[24] P. S. Krstić, C. O. Reinhold, and D. R. Schulz, J. Phys. B **31**, L155 (1998).
[25] K. G. Dyall, I. P. Grant, C. T. Johnson, F. A. Parpia, and E. P. Plummer, Comput. Phys. Commun. **55**, 425 (1989).
[26] M. O. Krause, J. Phys. Chem. Ref. Data **8**, 307 (1979).